Aging Cell (2011) **10,** pp239–254 Doi: 10.1111/j.1474-9726.2010.00658.x

Accelerated aging phenotype in mice with conditional deficiency for mitochondrial superoxide dismutase in the connective tissue

Nicolai Treiber,[1]* Pallab Maity,[1]* Karmveer Singh,[1]* Matthias Kohn,[1]* Alexander F. Keist,[1] Florentina Ferchiu,[1] Lea Sante,[1] Sebastian Frese,[2] Wilhelm Bloch,[2] Florian Kreppel,[3] Stefan Kochanek,[3] Anca Sindrilaru,[1] Sebastian Iben,[1] Josef Högel,[4] Michael Ohnmacht,[5] Lutz E. Claes,[5] Anita Ignatius,[5] Jin H. Chung,[6] Min J. Lee,[6] York Kamenisch,[7] Mark Berneburg,[7] Thorsten Nikolaus,[8] Kerstin Braunstein,[9] Anne-Dorte Sperfeld,[9] Albert C. Ludolph,[8,9] Karlis Briviba,[10] Meinhard Wlaschek[1] and Karin Scharffetter-Kochanek[1,8]

[1]Department of Dermatology and Allergic Diseases, University of Ulm, D-89081 Ulm, Germany
[2]Department of Molecular and Cellular Sports Medicine, German Sports University, D-50927 Cologne, Germany
[3]Department of Molecular Medicine, Division of Gene Therapy, University of Ulm, D-89081 Ulm, Germany
[4]Institute for Human Genetics, University of Ulm, D-89081 Ulm, Germany
[5]Institute of Orthopaedic Research and Biomechanics, University of Ulm, D-89081 Ulm, Germany
[6]Department of Dermatology, Seoul National University Hospital, Seoul 110-744, Korea
[7]Department of Dermatology, University of Tuebingen, D-72076 Tuebingen, Germany
[8]Competence Center for Gerontology and Aging Research, D-89081 Ulm, Germany
[9]Department of Neurology, University of Ulm, D-89081 Ulm, Germany
[10]Institute of Nutritional Physiology, Federal Research Centre for Nutrition and Food, D-76131 Karlsruhe, Germany

Summary

The free radical theory of aging postulates that the production of mitochondrial reactive oxygen species is the major determinant of aging and lifespan. Its role in aging of the connective tissue has not yet been established, even though the incidence of aging-related disorders in connective tissue-rich organs is high, causing major disability in the elderly. We have now addressed this question experimentally by creating mice with conditional deficiency of the mitochondrial manganese superoxide dismutase in fibroblasts and other mesenchyme-derived cells of connective tissues in all organs. Here, we have shown for the first time that the connective tissue-specific lack of superoxide anion detoxification in the mitochondria results in reduced lifespan and premature onset of aging-related phenotypes such as weight loss, skin atrophy, kyphosis (curvature of the spine), osteoporosis and muscle degeneration in mutant mice. Increase in $p16^{INK4a}$, a robust *in vivo* marker for fibroblast aging, may contribute to the observed phenotype. This novel model is particularly suited to decipher the underlying mechanisms and to develop hopefully novel connective tissue-specific anti-aging strategies.

Key words: Aging; connective tissue; mitochondria; $p16^{INK4a}$; reactive oxygen species; Sod2.

Introduction

Although reactive oxygen species (ROS) are part of normal regulatory circuits, imbalance or loss of cellular redox homoeostasis during aging results in oxidative stress (Sies, 1986, 1991), causing damage to cellular components. Apart from permanent genetic damage involving protooncogenes and tumour suppressor genes, ROS activate cytoplasmic signal transduction pathways that are related to growth, differentiation, tissue homoeostasis and senescence. Therefore, ROS have been implicated to play a causal role in tissue degeneration and – if deviant in composition and concentration – also in cancer and aging. Increased ROS concentration occurs in senescent fibroblast *in vitro* and *in vivo* (Scharffetter-Kochanek *et al.*, 1997; Allen *et al.*, 1999; Hutter *et al.*, 2002; Shin *et al.*, 2005). Fibroblasts constitute the principal component of the connective tissue. As such, fibroblasts occur in virtually every tissue and organ of the body. The capacity of fibroblasts to synthesize and organize the extracellular matrix and to communicate with other cells and tissues makes them a so far underestimated central component in organ homoeostasis and aging. Notably, the incidence of aging-related disorders such as skin- and muscle atrophy, osteoporosis and delayed wound healing are particularly high in connective tissue-rich organs including skin, bone and muscle causing major disability in the elderly. Skin aging is characterized by the loss of the elastic and collagen fibre network due to dysfunctional fibroblasts (Fisher *et al.*, 2008; Quan *et al.*, 2010) leading to wrinkle formation, reduced tensile strength and impaired

Correspondence
Karin Scharffetter-Kochanek, MD, Department of Dermatology and Allergic Diseases, University of Ulm, Maienweg 12, 89081 Ulm, Germany. Tel.: ++49 731 50057501; fax: ++49 731 50057502;
e-mail: karin.scharffetter-kochanek@uniklinik-ulm.de

Accepted for publication *13 November 2010*
*These authors contributed equally.

Aging Cell

wound healing. With aging, a progressive loss of skeletal muscle mass and strength occurs, a condition termed sarcopenia or muscle atrophy. Similar to skin atrophy and the loss of bone mass in the elderly (osteoporosis), muscle atrophy is a universal characteristic of the aging process in several species from worm to human (Fisher, 2004; Hiona & Leeuwenburgh, 2008). In older individuals, loss of muscle and bone mass is highly predictive of falls (Newton-John & Morgan, 1970; Szulc *et al.*, 2005), disability (Rantanen *et al.*, 1999) and mortality (Metter *et al.*, 2002). It leads to mobility disabilities with poor life quality and increased health care and social needs for the elderly (Iannuzzi-Sucich *et al.*, 2002). These pathological states share unique features and are all characterized by a loss of collagen type I, dysregulated fibroblast-matrix interactions and impaired fibroblast interactions with organ parenchyma, mainly with organ-specific epithelial cells and muscle (Wenk *et al.*, 1999, 2004; Krtolica & Campisi, 2002; Campisi, 2005; Labat-Robert & Robert, 2007; Treiber *et al.*, 2009). A variety of genetic and environmental factors including increased concentration of ROS, mitochondrial dysfunction (Hiona & Leeuwenburgh, 2008), changes in autocrine, paracrine and endocrine release of hormones, growth factors (Perrini *et al.*, 2010) and cytokines (Coppe *et al.*, 2008) have been identified to contribute to skin aging, sarcopenia and osteoporosis in humans and rodents (Zofkova, 2003; Raisz, 2005; Ralston & de Crombrugghe, 2006; Hiona & Leeuwenburgh, 2008; Marzetti *et al.*, 2009). Research on the regulation of connective tissue organization by enhanced release of ROS from mitochondria during fibroblast aging is a matter of increasing interest and relevance as it may provide ultimate clues for mechanisms underlying disruption of connective tissue homoeostasis in aging-related skin atrophy, sarcopenia and osteoporosis.

To protect against injury, aerobic cells, fibroblasts in particular have evolved a multilayered interdependent antioxidant system that includes enzymatic and non-enzymatic components. Among these Manganese superoxide dismutase (Sod2), a homotetramer, has been the subject of particular interest because it is located in the mitochondria and represents the first line of defence against superoxide radical mainly produced as by-product of oxidative phosphorylation. It converts superoxide radical into hydrogen peroxide, which is further detoxified to water by glutathione peroxidase and other peroxidases. Sod2 has earlier been identified as part of a phylogenetically conserved signalling pathway controlling aging and longevity at least in lower organisms (Kops *et al.*, 2002). Also, defined polymorphisms in the *Sod2* gene correlate with longevity and heart failure in elderly humans (Valenti *et al.*, 2004; Stessman *et al.*, 2005). However, due to early lethality in *Sod2* complete knock-out mice (Li *et al.*, 1995; Lebovitz *et al.*, 1996) and unchanged lifespan in mice heterozygous for the *Sod2* deficiency (Van Remmen *et al.*, 2003), the role of Sod2 and its specific requirements in distinct histogenetic compartments like the mesenchyme-derived connective tissues to prevent aging phenotypes have not yet been analysed. This information would be particularly important as connective tissue consists of resident mesenchyme-derived cells (e.g. fibroblasts) and extracellular matrix proteins, which are essential for organ function, its homoeostasis and most likely also for organismal aging. Most of the earlier studies investigate the effect of antioxidant enzymes deficiency or overexpression in all cells of transgenic mice for aging-related phenotypes (Muller *et al.*, 2007; Van Remmen & Jones, 2009). Even though these studies have provided valuable insight into aging-related disorders, they do not allow specifically investigating the impact of pro-oxidant connective tissue cells on skin, muscle and bone aging. This question is particularly interesting as fibroblasts revealed an accumulation of ROS during senescence *in vitro* and *in vivo* (Hutter *et al.*, 2002; Shin *et al.*, 2005) and given the ubiquitous distribution of fibroblasts in connective tissue stromas of all organs, it is likely that fibroblasts influence organ and organismal aging.

We have used a connective tissue-specific strategy to delete *Sod2* resulting in mutant mice. In contrast to mice with heterozygous *Sod2* deficiency in all organs (Van Remmen *et al.*, 2003; Strassburger *et al.*, 2005), we found a complex premature aging phenotype with skin atrophy, osteoporosis, muscle degeneration and a significantly reduced lifespan in the mutant mice. Fibroblasts in the skin of mutant mice revealed an increase in the expression of $p16^{INK4a}$, but did not undergo enhanced apoptosis, suggesting that atrophy in the skin, and most likely also in other organs, is due to the instalment of an oxidative damage-induced senescence programme.

Results

Generation of the mutant phenotype

To circumvent early lethality of *Sod2*-deficient mice (Li *et al.*, 1995; Lebovitz *et al.*, 1996; Strassburger *et al.*, 2005) and to address the impact of connective tissue-specific *Sod2* deficiency on aging of individual organs and lifespan, we have used a connective tissue-specific strategy with the introduction of loxP sites flanking exon 3 of the *Sod2* gene (Strassburger *et al.*, 2005). Deletion of exon 3 completely abrogates Sod2 activity, as exon 3 codes for the Sod2 tetramer formation domain (Li *et al.*, 1995). Mice carrying the floxed *Sod2* allele ($Sod2^{f/f}$) (Strassburger *et al.*, 2005) were bred with Col1α2-$Cre^{+}Sod2^{+/+}$ transgenic mice (Florin *et al.*, 2004) to generate Col1α2-$Cre^{+}Sod2^{+/f}$ mice. The connective tissue-specific Cre expression was achieved by the activation of α2(I) collagen promoter. While the above cross (first mating) resulted in a connective tissue-specific Cre expression, the second mating (Col1α2-$Cre^{+}Sod2^{+/f}$ x Col1α2-Cre^{-} $Sod2^{f/f}$) from the offspring of the first mating, due to transient Cre activation during gametogenesis in offspring of the first mating, resulted in mutant mice (mut) with connective tissue-specific homozygous deficiency for *Sod2* and a heterozygous deficiency for *Sod2* in all other organ parenchyma (Col1α2-Cre^{+} $Sod2^{-/f}$; Data S1 and Fig. S1, Supporting information). To assess specifically the impact of the connective tissue-specific homozygous lack of *Sod2* on aging, mutant mice (mut) were compared with mice revealing a heterozygous deficiency for *Sod2* in all organs (h) and to *Sod2*-competent mice (co) with

wild type levels of Sod2 activity. As we never observed differences between *Sod2*$^{+/+}$, Col1α2-Cre^{-}*Sod2*$^{+/f}$, Col1α2-Cre^{-}*Sod2*$^{f/f}$ and Col1α2-Cre^{+}*Sod2*$^{+/+}$ in phenotype nor in Sod2 activity, these genotypes were comparably used for experiments and were referred to as *Sod2*-competent control mice (co). Also, no difference in the Col1α2-Cre^{-} *Sod2*$^{-/f}$ and *Sod2*$^{+/-}$ was observed, and these genotypes were referred to as *Sod2* heterozygous mice (h).

Mutant mice reveal a progeroid phenotype and a decrease in lifespan

The mutant mice had a normal appearance until the age of 10–20 days, when a smaller size and reduced weight were first noted. As the mice got older, the kyphosis and decrease in size and weight became very obvious (Fig. 1a–c). Mutant mice have a progeroid appearance with a typical prominent forehead compared with *Sod2*-competent (co) mice (Fig. 1a). Reduction in length and weight occurred to a similar extent in female and male mutant mice (Fig. 1b,c) compared with *Sod2*-competent mice. A decrease in body weight was reported in human aging (Kalu, 1995) and is also well known in mice older than ~1.5 years (Haines *et al.*, 2001). The probability of survival decreased sharply during the first 4 weeks of life and thereafter decreased to a lesser extent (Fig. 1d), a finding most likely due to the mixed genetic background (Sv129 × C57BL/6J) of the mutant mice. No difference in lifespan was observed in *Sod2* heterozygous mice (h) compared with *Sod2*-competent mice (co, Fig. 1d), confirming previous data (Van Remmen *et al.*, 2003). The early dying mice can clinically be distinguished from late dying mutant mice by their almost complete immobility, their lack of feeding as controlled by metabolic cages (Fig. S2, Supporting information) and an increased rate of apoptosis in the hearts (Fig. S3, Supporting information). In contrast, the late dying mutant mice feed comparable quantities as control mice (Fig. S2, Supporting information) and did not reveal significantly increased apoptosis in the heart muscle (Fig. S3, Supporting information). In the following experiments, we have included only late dying mutant mice (> 100 days), as the early dying mutant mice (< 100 days) may not represent a convincing aging model, but may be more pertinent to a disease model.

Accelerated aging phenotype in muscle, bone and skin of mutant mice

A motor phenotype with progressive limb clasping consistently occurred upon tail suspension in mutant mice (mut, 30/32)

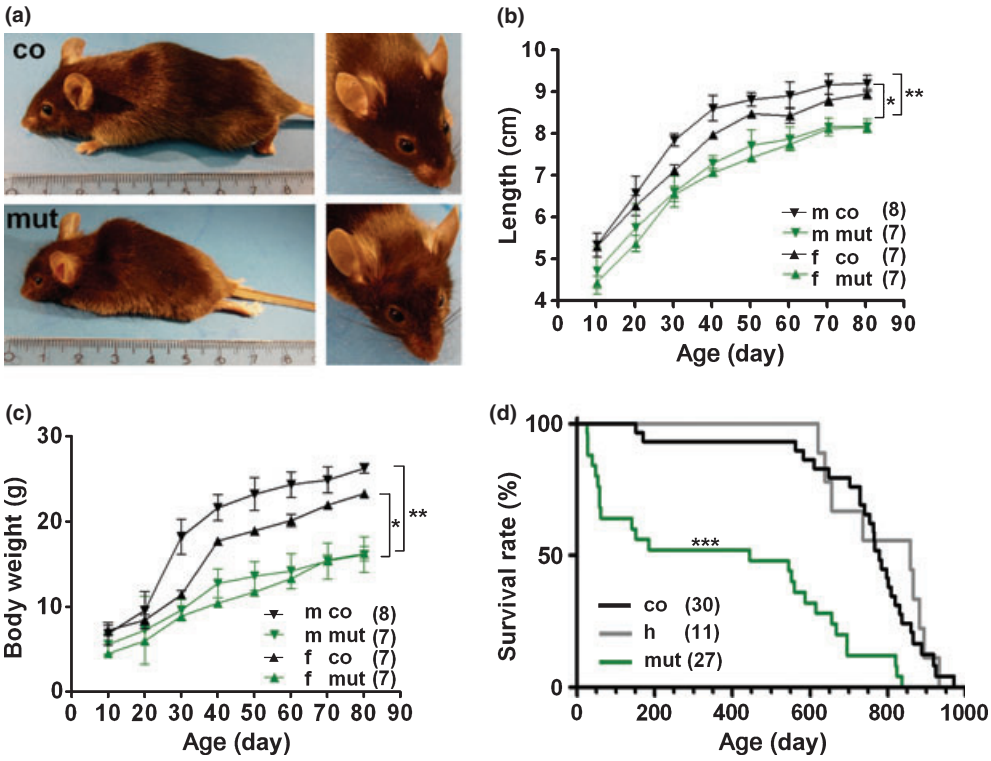

Fig. 1 Progeroid gross appearance and decrease in lifespan in mutant mice. (a–c) The mutant mice (mut) at an age of 150 days revealed kyphosis and a prominent progeroid forehead compared with littermates of *Sod2*-competent (co) mice (a), reduced body size (b) and weight (c). Female controls (f co) vs. female mutant mice (f mut), **P* = 0.005, male controls (m co) vs. male mutant (m mut) mice, ***P* = 0.003 (after Bonferroni correction). All error bars indicate standard deviation. (d) Significantly reduced survival time of mutant mice (median 444 days) compared with *Sod2*-competent control mice (median 784 days) (****P* < 0.0001, log-rank test stratified for gender). No statistically significant difference was found between *Sod2*-competent (co) and *Sod2* heterozygous (h) mice (*P* = 0.65). The maximal lifespan for mutant mice was 837 days compared with 971 days in *Sod2*-competent mice and 932 days in *Sod2* heterozygous mice.

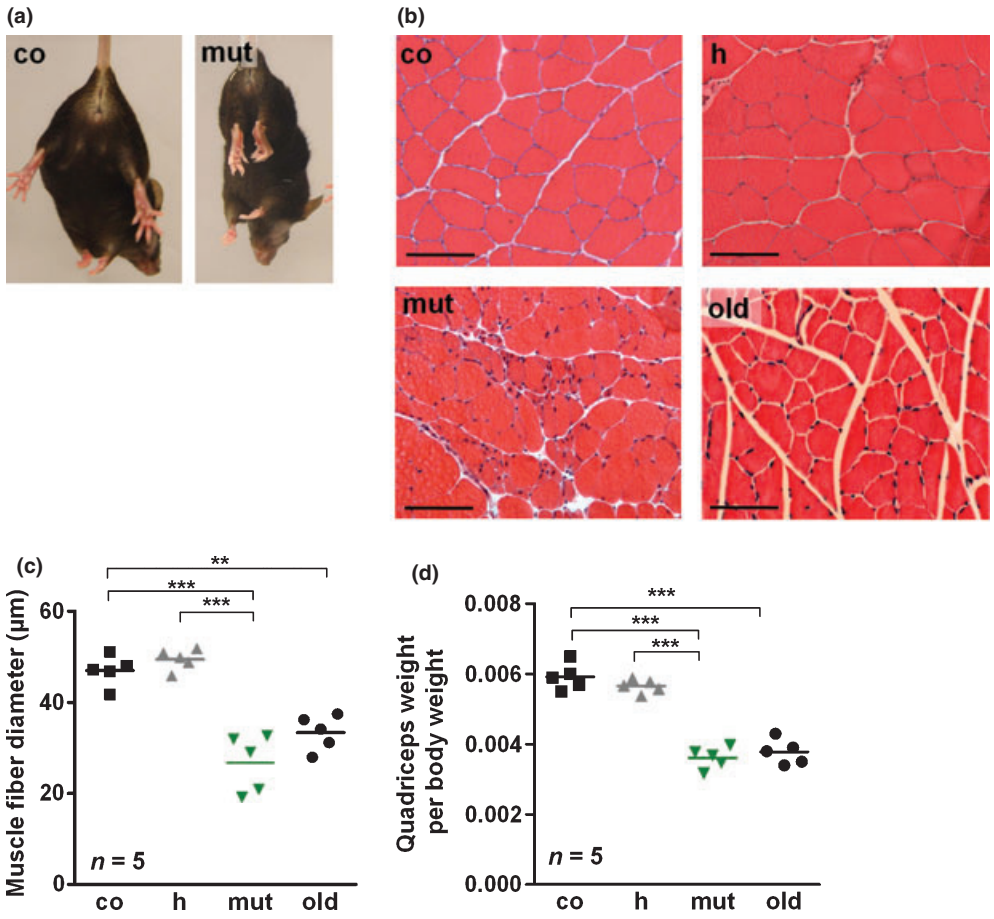

Fig. 2 Motor phenotype and muscle atrophy in mutant mice. (a) Mutant mice at ages ranging from 100 days to > 600 days revealed clasping of hind limbs (indicating deficits in motor coordination) (mut, 30/32), whereas *Sod2*-competent mice (co, 0/40) at the same age exhibited normal hind limb extension upon tail suspension. (b) Representative haematoxylin-eosin stained sections of the quadriceps muscle revealed muscle atrophy in mutant mice (mut, 150 days), and intrinsically aged mice (old, 900 days), Compared with the normal muscle architecture in *Sod2* heterozygous-deficient (h, 150 days) and *Sod2*-competent mice (co, 150 days). (c) Diameters of skeletal muscle derived from mutant mice (mut) and intrinsically aged mice (old, 900 days) were significantly reduced compared with *Sod2*-competent (co) and *Sod2* heterozygous (h) mice at an age of 150 days. Observations and the mean value are shown (co/h vs. mut, ***$P < 0.001$, co vs. old **$P < 0.01$ after Bonferroni correction). Scale bars, 20 µm. (d) Ratio of quadriceps muscle weight to body weight (co/h vs. mut, ***$P < 0.001$, co vs. old **$P < 0.001$, after Bonferroni correction).

compared to no clasping in *Sod2*-competent (co, 0/40) and *Sod2* heterozygous mice (h, 0/40) (Fig. 2a). This limb clasping was progressive and more severe in older animals. Testing motor coordination and balance by means of the rotarod test, mutant mice revealed a severe phenotype with only 50% performance (5/5) compared with mice of either *Sod2* heterozygous or *Sod2*-competent genotype (data not shown). Histology revealed a large reduction in the diameters of muscle fibres and high variability of fibre size indicating a severe muscle cell atrophy in mutant mice (mut, 5/5, 150 days) compared with aged-matched *Sod2*-competent (co, 0/5) and *Sod2* heterozygous littermates (h, 0/5) (Fig. 2b, c). Variability of fibre size and reduction in diameter of muscle fibres were also found in intrinsically aged control mice of 900 days (old) (Fig. 2c). In addition, transverse sections of skeletal muscle from Sod2 heterozygous and competent mice did not reveal gross differences in morphology (Fig. 2b,c). The ratio of quadriceps mass (weight) to body weight revealed a reduction in muscle mass in mutant (150 days) and intrinsically aged control mice (900 days), but not in heterozygous-deficient mice (150 days) and littermate control mice of the same age (Fig. 2d). These data indicate that the reduced muscle fibre diameter is due to muscle atrophy and not simply to overall reduced body weight. Notably, similar to intrinsically aged control mice (900 days), a severe osteoporosis-like phenotype was found in mutant mice (150 days) as quantitative assessment with X-ray densitometry of femur bones revealed a dramatic decrease in the mineral density in mutant mice (mut, 5/5) compared with *Sod2*-competent mice (co, 0/5) of the same age (Fig. 3a). In addition, severe skin atrophy was detected in mutant (150 days) and old mice (900 days), but not in *Sod2* heterozygous-deficient mice compared with *Sod2*-competent mice at the same age of 150 days (Fig. 3b and Fig. S4, Supporting information). Histologically, mutant mice showed severe skin atrophy in the dermal and the subcutaneous compartment with reduced vertical diameter (5/5) compared with no or less atrophy in *Sod2* heterozygous-deficient (5/5) and con-

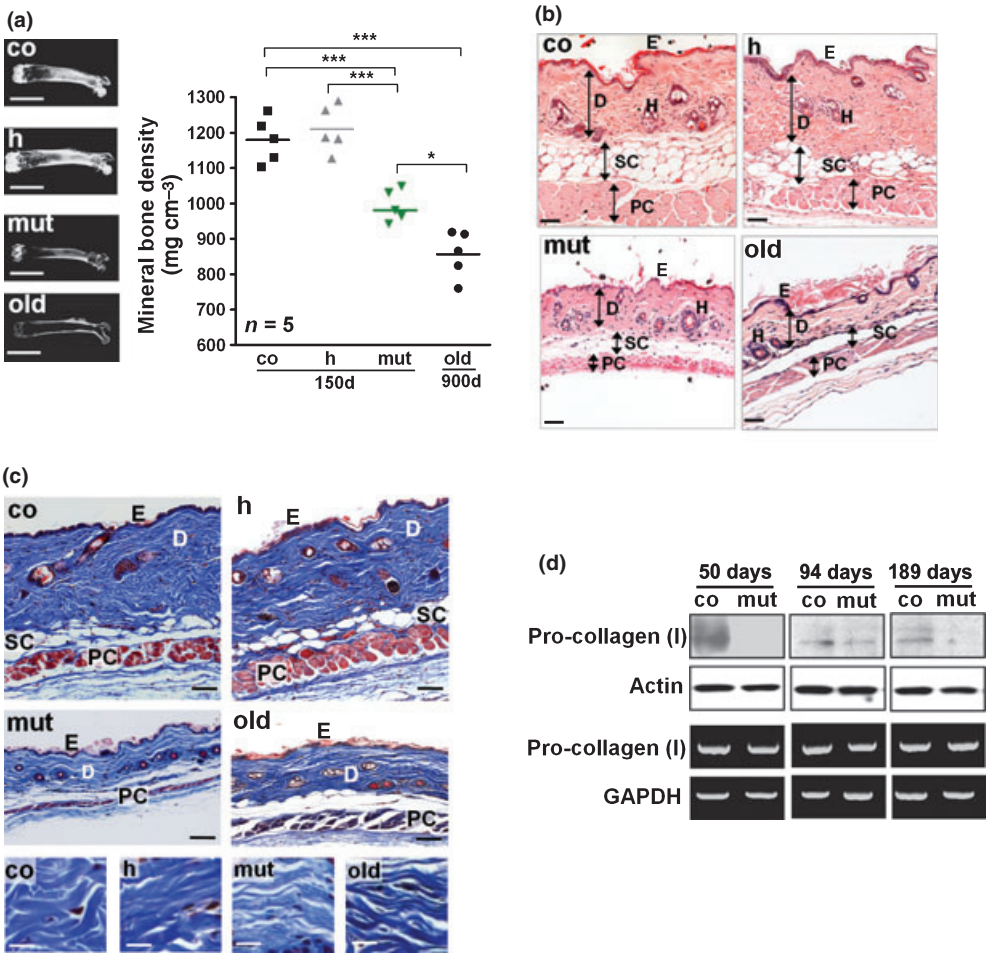

Fig. 3 Osteoporosis-like phenotype and skin atrophy in mutant mice. (a) X-ray analysis (left panel) and bone density (right panel) from dissected femur bone of *Sod2*-competent mice (co), *Sod2*-heterozygous mice (h), mutant mice (mut) and intrinsically aged mice (old) revealed an osteoporosis-like phenotype in mutant mice (co/h vs. mut, ***$P < 0.001$; after Bonferroni correction) and old mice (co vs. old, ***$P < 0.001$; after Bonferroni correction). Scale bars, 0.5 cm. co, h, mut mice were studied at an age of 150 days and intrinsically aged mice at an age of 900 days (old). (b) Mutant mice at an age of 150 days revealed a severe atrophy of the dermis, the subcutaneous fat tissue and the muscle fibres of the panniculus carnosus compared with *Sod2*-competent mice. Only minor changes in *Sod2* heterozygous-deficient mice at the same age were evident compared with *Sod2*-competent mice. Intrinsically aged mice of 900 days (old) revealed a similar phenotype as mutant mice. Representative haematoxylin-eosin stained sections of the skin. E, epidermis; D, dermis; H, hair follicle; SC, subcutaneous fat tissue; PC, panniculus carnosus. Scale bars, 20 μm. (c) Representative Masson's trichrome staining revealed an altered organization and reduced thickness of collagen fibres and the dermal connective tissue in all mutant mice (mut, 6/6) at an age of 150 days and intrinsically aged (old, 900 days, 3/3) mice compared with the normal architecture of the dermis in *Sod2*-competent controls (co, 5/5) and heterozygous-deficient (h) mice at an age of 150 days. Collagen fibres of *Sod2*-competent (co), heterozygous (h), mutant (mut) and intrinsically aged (old) mice are shown at higher magnification (lower left panel). Higher magnification of Masson's trichrome staining of dermal collagen fibres in *Sod2*-competent control (co) and *Sod2* heterozygous (h)-deficient mice revealed densely packed thick fibres. In contrast, in mutant and old mice, collagen fibrils are thinner and loosely organized. E, epidermis; D, dermis; SC, subcutaneous fat tissue; PC, panniculus carnosus. Scale bars, 20 μm for overview and 5 μm for magnified view. (d) Western blot analyses of skin lysates with antibodies directed against pro-collagen type I (upper panel) revealed a significant decrease in pro-collagen type I in mutant mice (mut) at different ages (50, 94, and 189 days) compared with age-matched *Sod2*-competent controls (co). Actin served as a loading control. Semi-quantitative RT-PCR of pro-collagen type I mRNA isolated from the dermis of mutant mice (mut) and *Sod2*-competent mice (co) at different ages (lower panel) as indicated above. GAPDH served as housekeeping gene and loading control.

trol mice (5/5) (Fig. 3b and Fig. S4, Supporting information). In addition, also the muscular layer of the panniculus carnosus in the skin is atrophic with reduced vertical diameter (5/5). Similar results were found in intrinsically aged mice of > 900 days (Fig. 3b and Fig. S4, Supporting information).

To study the impact of *Sod2* deficiency of fibroblasts in the skin, deposition of collagen and collagen fibril organization were assessed. Using Masson's trichrome staining for collagen, the atrophy of the dermis as indicated by reduced vertical thickness of the dermis in the mutant mice (mut) (Fig. 3c, left middle panels) compared with *Sod2*-competent (co) littermates was confirmed (Fig. 3c left upper panel). Mice with a *Sod2* heterozygous deficiency (h) (Fig. 3c, upper right panel) did not differ from control mice (co). In addition, skin of intrinsically aged (old) mice of 900 days (Fig. 3c, middle right panel) revealed a similar atrophy of the dermis as found in mutant mice. The lower panel (Fig. 3c) depicted that virtually no difference in thickness and density of collagen fibres occurred in control mice when compared with *Sod2* heterozygous-deficient mice. Notably, smaller collagen fibres loosely arranged in less density were observed

both in mutant mice and in old mice. Western blot analysis of skin lysates of mice at different ages revealed a significant decrease in collagen type I [$\alpha_1(\alpha_2)_2$I] to almost undetectable levels in mutant mice (Fig. 3d). Interestingly, specific collagen mRNA levels did not differ in mutant and Sod2-competent mice suggesting that the decrease in collagen deposition occurs at the translational and/or posttranslational level (Fig. 3d).

Deletion of Sod2 is fibroblast-specific in different organs of mutant mice

Crossing the *Sod2* floxed mice with ROSA26-LacZ reporter mice, revealed β-galactosidase expression only in interstitial fibroblasts in different organs (Fig. S5, Supporting information). To show specific Sod2 deficiency in the connective tissue resident fibroblasts in skin and skeletal muscle, we performed double staining with an antibody against Sod2 and an antibody directed against a fibroblast-specific intracellular epitope of reticulin (Er-TR7) which previously has been successfully used to define the microarchitecture of organs (Petrie & Van Ewijk, 2002; Kim *et al.*, 2009). Expectedly, skin and muscle (Fig. S6, Supporting information) from control mice revealed double staining exclusively in fibroblasts when merged, while all other cells in skin and muscle fibres stained for Sod2. In contrast, in the skin of mutant mice, exclusive ER-TR7 positive staining was observed in fibroblasts, while no staining for Sod2 was detected. The epidermis, hair follicles and the muscle layer of the panniculus carnosus of the skin, as well as skeletal muscle fibres revealed a clear staining for Sod2 in the mutant mice. These data indicate a connective tissue-specific lack of Sod2 in fibroblasts studied in the skin and skeletal muscle (Fig. S6, Supporting information) and other organs (data not shown).

Mutant mice reveal oxidative damage and a premature increase in aging-related *in vivo* biomarkers

Using Western blot analysis, we confirmed the lack of Sod2 in mutant fibroblasts (Fig. 4a). The lack of Sod2 in mutant fibroblasts led to an increase in superoxide anion concentration (Fig. 4b) ($P < 0.05$), as measured by indirect fluorescence with the mitochondrion-specific superoxide anion indicator, MitoSOX. Adenovirally transduction of the HyPer construct was used to visualize specifically changes in H_2O_2 levels in the mitochondria of *Sod2*-deficient and competent fibroblasts. A reduction of mitochondrial H_2O_2 in *Sod2*-deficient fibroblasts compared with *Sod2*-competent fibroblasts was found (Fig. 4c) ($P < 0.05$). Lack of Sod2 in fibroblasts led to severe structural changes in 80% of the mitochondria with loss of cristae and degeneration, with > 60% intact mitochondria in *Sod2* heterozygous and 95% intact mitochondria in *Sod2*-competent fibroblasts (Fig. 4d). Oxidative damage of protein as detected by carbonylation, was consistently increased in lysates of dermal fibroblasts from mutant mice, compared with *Sod2*-competent fibroblasts (Fig. 4e) and heterozygous fibroblasts (data not shown).

Increase in superoxide anion concentrations, as is the case in mutant mice, may induce oxidative DNA damage and DNA double strand breaks. This can activate cell cycle check points through p21 or p53, and subsequently results in growth arrest of cells harbouring DNA damage. Alternatively, a cellular senescence programme can be activated by DNA double strand breaks, resulting in irreversible p16-mediated cellular growth arrest. Cell cycle arrest thus prevents that the damaged DNA becomes mutagenic for daughter cells (for review see Campisi, 2005). We did not find any upregulation of p21 and p53 (data not shown). However, fibroblasts in the skin of mutant mice at ages ranging from 150 to 550 days revealed high expression of $p16^{INK4a}$ (Fig. 5a, b), a cell cycle inhibitor, which not only mediates the DNA damage response to the senescence state with induction of growth arrest, but also constitutes a robust *in vivo* biomarker for aging of different organs including the skin (Krishnamurthy *et al.*, 2004; Ressler *et al.*, 2006). Enhanced $p16^{INK4a}$ expression was also found in the skin of intrinsically aged control mice of 700 and 900 days (Fig. 5b). Western blot analysis showed a slight increase in $p16^{INK4a}$ in the skeletal muscle of mutant mice at the age of 300 days compared with Sod2 control mice at the same age (Fig. 5b). In contrast, apoptosis of resident fibroblasts in the dermis of 150 days old mutant mice did not differ significantly compared with *Sod2*-competent mice, as revealed by 'Terminal deoxynucleotidyl' transferase dUTP nick end labelling (TUNEL) and active caspase-3 immunostaining (Fig. 5c, d). Also Western blot analysis did not show any difference in the activation of caspase-3 in skin lysates of mutant mice at an age of 150 and 550 days (data not shown), indicating that apoptosis is not enhanced in the dermis of mutant mice.

Discussion

Here, we have shown for the first time that connective tissue-specific lack of superoxide anion detoxification resulted in a reduced lifespan and premature onset of aging-related phenotypes, such as weight loss, skin atrophy, kyphosis, osteoporosis and muscle degeneration. This is most likely due to oxidative damage-induced activation of a senescence programme with overexpression of $p16^{INK4a}$ and irreversible growth arrest of connective tissue-associated fibroblasts with substantially reduced collagen deposition and impaired interaction with interstitial collagen fibrils, the major structural component of the extracellular matrix in the skin, bone and muscle.

Our major finding is that selective loss of redox balance in connective tissue resident fibroblasts is sufficient to drive such a complex aging phenotype in different organs and to shorten lifespan. In fact, the mice with a heterozygous *Sod2* deficiency did not reveal this severe progeroid phenotype in all studied aspects. This is further supported by few independent publications, which did not report a reduced lifespan, bone or muscle phenotype in mice with heterozygous *Sod2* deficiency (Van Remmen *et al.*, 2003; Strassburger *et al.*, 2005). We observed a bimodal shape of the lifespan, with early dying mice during the first weeks after birth and late dying mutant mice, which

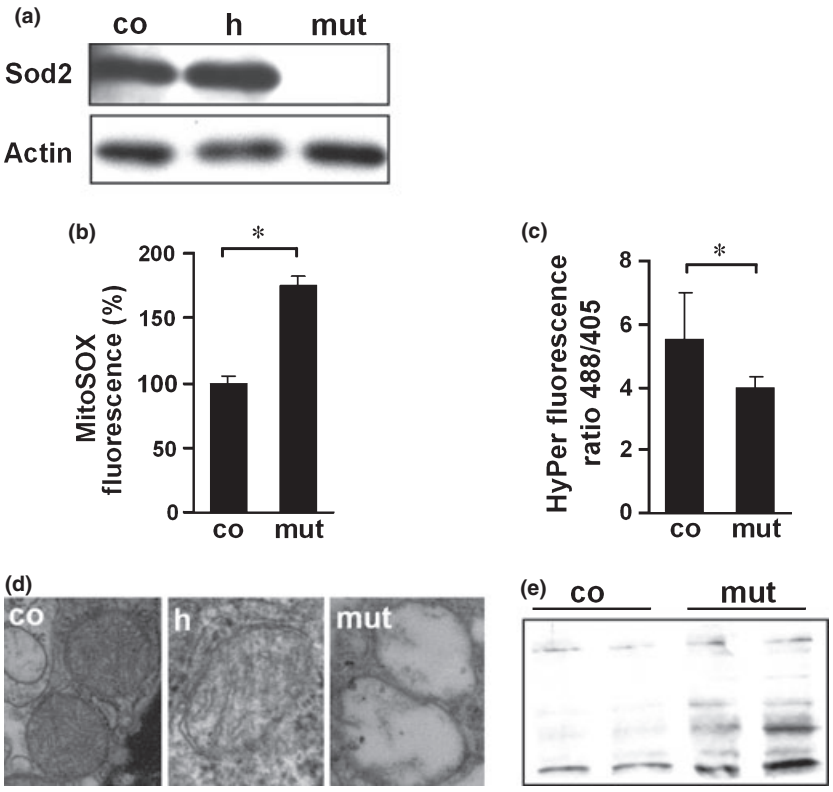

Fig. 4 Oxidative damage, accumulation of superoxide anion and decrease in hydrogen peroxide in skin fibroblasts of mutant mice. (a) Representative Western blot analysis of skin fibroblast lysates derived from the *Sod2*-competent (co), heterozygous (h) and mutant mice (mut) were probed with an anti Sod2 antibody. Actin was used as loading control. (b) Superoxide anions in fibroblasts were quantified using indirect fluorescence with MitoSOX. MitoSOX is mitochondrion-specific, and the reaction of superoxide anions with this dye caused fluorescence emission. Fibroblasts from mutant mice revealed a significantly higher fluorescence emission compared with *Sod2*-competent mice, indicating an accumulation of superoxide anion in the mitochondria of mutant mice. Data are expressed as percentage of mean ± standard error of mean, (*$P < 0.05$ co vs. mut). The experiment shown here is representative of three independent experiments. (c) Fibroblasts from control and mutant mice were adenovirally transduced with the construct of mitochondrially targeted HyPer (Ad Mito-HyPer) and subjected to FACS analysis for quantification of HyPer oxidation in the mitochondria as a measure of defined H_2O_2 levels. Fluorescence intensities of AdMito-HyPer in mutant fibroblasts and *Sod2*-competent fibroblasts were measured following activation by 488 and 405 nm and expressed as fluorescence ratio 488/405 as indicated in Materials and Methods, comparing fluorescence ratio of mutant fibroblasts with *Sod2*-competent fibroblasts. Data indicate that H_2O_2 levels are significantly reduced in mutant compared with *Sod2*-competent fibroblasts (*$P < 0.05$). The data are expressed as mean ± standard error of mean. Three independent experiments were performed in triplicates with a representative experiment shown here. (d) Transmission electron microscopy and assessment of 100 mitochondria revealed a severely disturbed structure with loss of cristae and degeneration of intramitochondrical structure in > 80% of all assessed mitochondria in mutant fibroblasts (mut) compared with 40% damaged mitochondria in *Sod2* heterozygous (h) and only 5% in *Sod2*-competent fibroblasts (co). Similar data were found in three additional mice of each genotype in the dermis. Representative mitochondria are shown for each genotype. (e) Oxyblots were performed with lysates from dermal fibroblasts of mutant (mut) and *Sod2*-competent mice (co) with significantly enhanced general protein carbonylation indicative of oxidative damage in all mutant mice (mut, 3/3) compared with less carbonylation in *Sod2*-competent mice (co, 3/3). Two independent lysates of the competent and mutant genotype are shown.

revealed a reduced lifespan compared with control mice. Several reasons including segregation of modifier genes or replicative segregation of mutant mitochondrial DNA or a combination thereof may contribute to the early death of the mutants and to the bimodal shape of the lifespan curve in the mutant mice. The studied mutant mice are on a mixed background derived from C57BL/6J and SV129/ola inbred strains. Interestingly, genetic modifiers of lifespan of mice deficient in Sod2 have earlier been reported (Huang *et al.*, 2006). The gene encoding nicotinamide nucleotide transhydrogenase (Nnt) was found to be one of such modifiers in the C57BL/6J mice, where this gene is mutated and functional Nnt protein could not be detected. Nnt is a nuclear encoded mitochondrial inner membrane protein which couples the generation of NADPH to proton transport and provides NADPH for the generation of two important antioxidants (glutathione and thioredoxin) in the mitochondria. If non-functional as in the C57BL/6J background, the mutant Nnt could contribute to the lifespan shortening in Sod2-deficient mice (Huang *et al.*, 2006). To test the possibility that the early dying mutants in our study reveal a mutation in the *Nnt* gene, we systematically screened for this mutation. However, we did not detect any correlation with lifespan shortening and the Nnt mutation in the early dying mutants (data not shown). This does not, however, exclude the segregation of other so far unknown modifier genes responsible for shortening of the lifespan in early dying mutant mice. In addition, the stochastic and quantitative nature of mitochondrial DNA genetics is known to result in a highly variable inheritance and expression of heteroplasmic mutations (Wallace

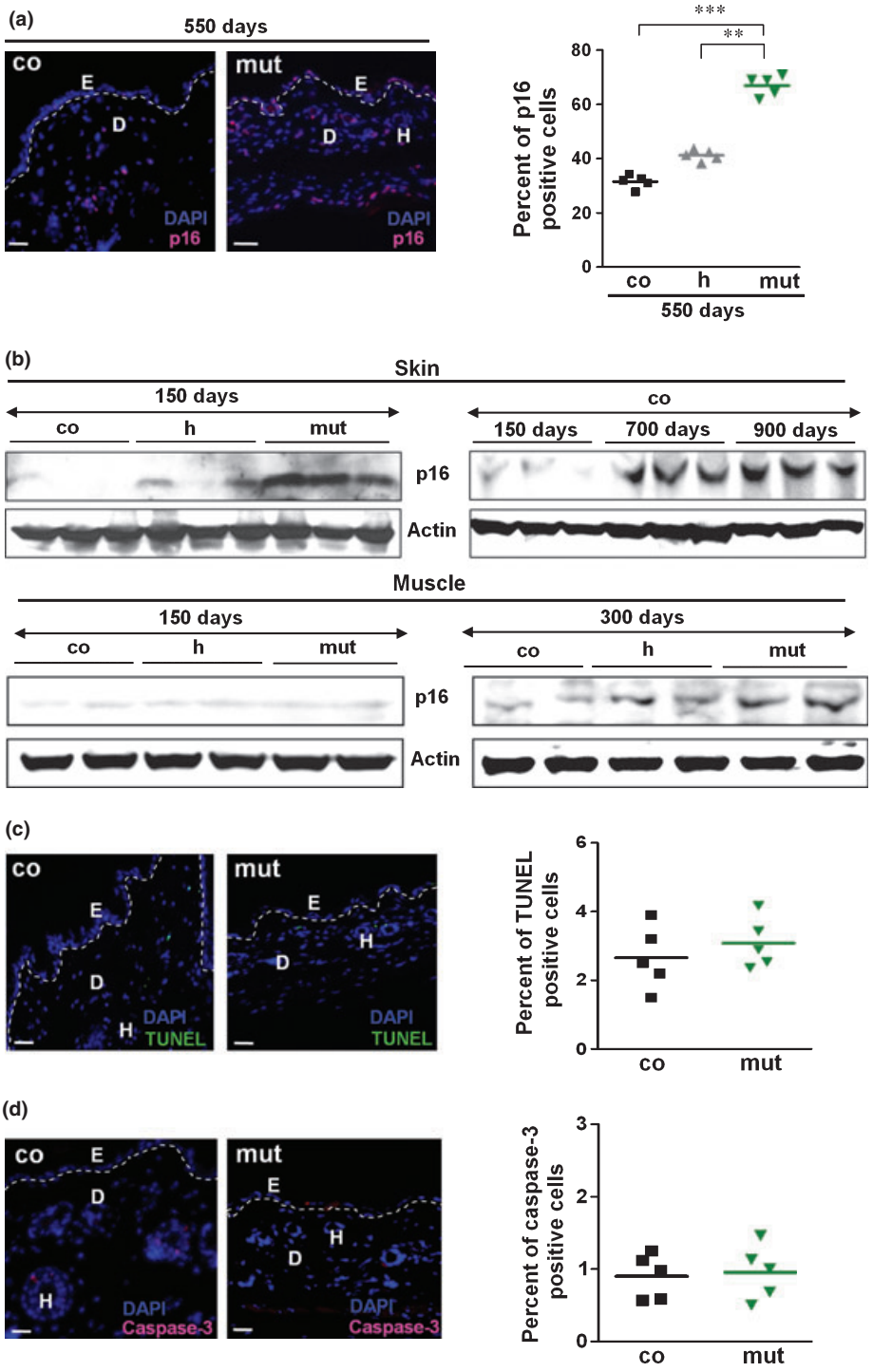

Fig. 5. Oxidative damage resulted in the induction of the senescence marker $p16^{INK4a}$ in mutant mice. (a) Immunostaining with antibodies against $p16^{INK4a}$, an established aging marker, was significantly increased in the dermal connective tissue of all mutant mice at an age of 550 days (mut, 5⁄5) compared with *Sod2* heterozygous (h, 0⁄5) and *Sod2* compentent (co, 0⁄5) at the same age of 550 days. $p16^{INK4a}$ was stained in red (Alexa 555) and nuclei in blue (DAPI). Immunostaining of the skin and the mean value of $p16^{INK4a}$ positive cells are shown (co vs, mut, $***P < 0.001$, h vs, mut $**P < 0.01$ after Bonferroni correction). E, epidermis; D, dermis; H, hair follicle. Scale bars, 20 μm. (b) Upper left panel shows Western blot analysis of $p16^{INK4a}$ in skin lysates of 150 days old co, h and mut mice. Upper right panel shows Western blot analysis of $p16^{INK4a}$ in skin lysates of 150, 700 and 900 days old control mice. Left third panel shows Western blot analysis of $p16^{INK4a}$ in skeletal muscle lysate of 150 days old co, h and mut mice and right third panel shows Western blot analysis of $p16^{INK4a}$ in skeletal muscle lysates of 300 days old co, h and mut mice. Actin served as loading control for the $p16^{INK4a}$ Western blot. (c) 'Terminal deoxynucleotidyl' Transferase dUTP nick end labelling (TUNEL) assay (left panel) of skin sections and quantification of TUNEL positive cells (right panel) did not reveal any significant difference in apoptosis in the skin of *Sod2* mutant (150 days) compared with control mice of the same age. (d) Immunostaining with antibodies against cleaved (active) caspase-3 indicative of apoptotic cells was performed on skin sections (left panel) and was quantitatively assessed (right panel). No significant difference was observed between *Sod2*-competent (co) and mutant mice (mut) at an age of 150 days.

et al., 1999; Wallace, 2010) and thus may contribute to the bimodal shape of the lifespan curve in the herein described mutant mice.

The mutant mice with a complete *Sod2* deficiency in sarcolemmal fibroblasts in close proximity to the muscle fibres with a heterozygous *Sod2* deficiency, showed a severe muscle atrophy in terms of decreased fibre diameter, increased variability and a significantly decreased muscle mass to body weight ratio, accepted hallmarks of muscle atrophy in intrinsically aged rodents and humans (Larsson, 1978; Usuki *et al.*, 2004). In contrast, mice with a heterozygous *Sod2* deficiency throughout all organs including sarcolemmal fibroblasts and muscle fibres themselves did not show any muscle atrophy and could not be distinguished from muscle fibres of *Sod2*-competent littermate controls. Therefore, given that homozygosity for the *Sod2* deficiency in fibroblasts represents the only difference between *Sod2*-deficient heterozygous and mutant mice, it is tempting to suggest a scenario where the complete *Sod2* deficiency in fibroblasts of the sarcolemmal connective tissue, which ensheat each muscle fibre, may significantly contribute to the observed severe muscle atrophy. The muscle fatigability and the observed pathological motor phenotypes in mutant mice as suggested by the data from rotarod and tail suspension test, mostly likely originate from the impairment of the muscle architecture. These observed changes have earlier been described in old rodents (Usuki *et al.*, 2004) and human muscle (Larsson, 1978). However, we cannot exclude that disruption of the neuromuscular junction may have some influence on the observed motor phenotype of the mutant mice as previously published in mice deficient for the Cu, Zn superoxide dismutase (Jang *et al.*, 2010). Serial sections of the spinal cord with α-motor neurons and neurons from the cerebral cortex did not reveal any morphological changes (data not shown). This, in conjunction with the observed severe muscle atrophy, provides evidence that the mutant mice rather suffer from a progressive aging-related muscle atrophy.

This is further supported by preliminary data on Tamoxifen inducible connective tissue-specific *Sod2* deletion (data not shown), where the *Sod2* deficiency exclusively occurred in fibroblasts, but not in muscle fibres. Several reasons may contribute to the effects of *Sod2*-deficient fibroblasts on the development of severe muscle atrophy observed in the mutant mice. Accordingly, $Sod2^{-/-}$ fibroblasts from mutant mice may affect skeletal muscle cells by changes in the quality and quantity of extracellular matrix proteins, soluble paracrine factors including catabolic cytokines, growth factors (Coppe *et al.*, 2008) or long-lived toxic lipid peroxidation products due to enhanced superoxide anion generation. Given the fact that fibroblasts are in close proximity to skeletal muscle cells, their impact on the microenvironment of skeletal muscle cells is critical. Age-related oxidative damage, lipid peroxidation and mitochondrial protein damage in murine skeletal muscle have previously been reported (Lass *et al.*, 1998). Irrespective of the underlying mechanisms, we have shown that *Sod2* homozygous deficiency in sarcolemmal fibroblasts in close proximity to muscle fibres can tilt the biological outcome to muscle atrophy. This may be of relevance to human aging and aging-related pathologies as, similar to the here reported mutant model, senescent human fibroblasts reveal increased superoxide anion concentrations (Fig. S7, Supporting information).

Similarly, osteoporosis and skin atrophy belong to universal aging-related phenotypes in mice and humans leading to major disability in the elderly. We have found a severe decrease in mineral density in femur and vertebrae bone in mutant mice (150 days) and intrinsically aged mice (900 days), but not in *Sod2* heterozygous-deficient and *Sod2*-competent control mice at an age of 150 days. Consistent with our data, a similar decrease in mineral density in both vertebrae and femur bone was earlier reported in intrinsically aged mice (Kalu, 1995). Kyphosis (curvature of the spine), as observed in the mutant and intrinsically aged mice, may be linked to osteoporosis with loss of trabecular bone in vertebral bodies of the middorsal spine or to muscle atrophy (Gerhard & Kasales, 2003) or a combination thereof, as most likely in our model. In humans, osteoporosis causes kyphosis through the deformity of the vertebral bodies (Cummings & Melton, 2002). The current concept suggests that osteoporosis represents a continuum with multiple underlying mechanisms contributing to loss of bone mass and mineral density and overall microarchitectural deterioration of bones (Ferrari *et al.*, 2004; Tasker *et al.*, 2004; Bodine *et al.*, 2005; Horowitz & Lorenzo, 2007; Perrini *et al.*, 2010). These factors are causally related to increased risk of falls, contributing to high incidence of fragility fractures in osteoporotic patients (Raisz, 2005; Ralston & de Crombrugghe, 2006).

Similar to the bone and muscle atrophy, also the skin is atrophic in mutant mice and intrinsically aged mice. A comparable skin atrophy in intrinsically aged mice and humans has repeatedly been reported (Oikarinen, 1994; Scharffetter-Kochanek *et al.*, 1997; Kaya *et al.*, 2006). As expected, dermal fibroblasts from mutant mice revealed an increase in superoxide anion concentration and a decrease in hydrogen peroxide concentration in the mitochondria. This led to the development of oxidative damage and finally to the degeneration of mitochondria. Both collagen deposition and fibril thickness are severely reduced in the dermis of the skin. Collagen type I, the most abundant matrix protein in the skin, was severely reduced at the protein level in the skin of mutant mice. As the specific collagen type I mRNA concentrations are similar in mutant mice compared with control mice, either increased collagen degradation by matrix-metalloproteases or reduced biosynthesis at a post-transcriptional level are responsible for the observed reduction in collagen deposition in the skin of mutant mice. Both reduction in collagen synthesis and induction and activation of matrix-degrading metalloproteases are critical in human skin aging (Ma *et al.*, 2001; Shin *et al.*, 2005).

The connective tissue-specific *Sod2*-deficient model sharing murine and human aging-related pathologies is particularly interesting to unravel the underlying mechanisms. Due to *Sod2* deficiency and a lack of superoxide anion detoxification, the concentration of superoxide anion increased in mutant fibroblasts as shown herein. Superoxide anions and intermediates thereof

like peroxynitrite can severely damage macromolecules, and most importantly, they can induce DNA double strand breaks and intercrosslinks in the DNA (Szabo *et al.*, 2007). Such lesions usually promote apoptosis or induce a senescence programme with permanent growth arrest contributing to organ atrophy and most likely to organismal aging (Niedernhofer *et al.*, 2006; van der Pluijm *et al.*, 2007; Garinis, 2008; Garinis *et al.*, 2008). We did not find induced apoptosis in the connective tissue of *Sod2* mutant mice compared with *Sod2*-competent wild type control. Notably, we found that the cell cycle inhibitor $p16^{INK4a}$ time-dependently increased in the dermal and muscle connective tissue of mutants, while there was significantly less $p16^{INK4a}$ expression in *Sod2* heterozygous-deficient and *Sod2*-competent mice. $p16^{INK4a}$ constitutes a major player in the instalment of a ROS/DNA damage-induced senescence programme (Dai & Enders, 2000; Kim & Sharpless, 2006). In this regard, $p16^{INK4a}$ functions as an inhibitor of CDK4 and CDK6, the D-type cyclin-dependent kinases that initiate the phosphorylation of the retinoblastoma tumour suppression protein RB. Thus, $p16^{INK4a}$ has the capacity to arrest cells in the G1 phase of the cell cycle implementing irreversible growth arrest. The fact that the expression of the $p16^{INK4a}$ increases markedly with aging in many tissues of rodents and humans (Krishnamurthy *et al.*, 2004, 2006; Molofsky *et al.*, 2006; Ressler *et al.*, 2006) very much suggests that our mutant mouse model distinctly shares mechanisms underlying intrinsic aging.

Our model with preferential oxidative damage of fibroblasts residing in the connective tissue of different organs may very well reflect the situation in patients subjected to ROS and DNA damage-inducing chemotherapy or radiotherapy (Grillari *et al.*, 2007). While tissues with highly proliferative cells of epithelial origin mainly undergo apoptosis, connective tissue resident fibroblasts rather undergo a senescence programme with a metabolically changed phenotype, loss of tissue homoeostasis and aging. In fact, long-term survivors of chemotherapy and radiotherapy show evidence for premature aging (Grillari *et al.*, 2007).

The herein reported mutant mice sharing universal murine and human age-related changes are particularly interesting to unravel the underlying mechanisms and to identify strategies to counteract accelerated aging.

Experimental procedures

Generation of mutant mice

Mice carrying the homozygous floxed *Sod2* allele ($Sod2^{f/f}$; B6;129.$Sod2^{tm1Ksk}$) (Strassburger *et al.*, 2005) were bred with Col1α2-Cre^{+} transgenic mice (B6;129.TgN(Col-Iα2) (Florin *et al.*, 2004) to generate Col1α2-$Cre^{+}Sod2^{+/f}$ mice. In a second mating, this mouse (Col1α2-$Cre^{+}Sod2^{+/f}$) line was bred to homozygous $Sod2^{f/f}$ mice to obtain connective tissue-specific *Sod2*-deficient offspring. The resulting transgenic mice (B6;129.$Sod2^{tm1.1Ksk}$) were of a mixed genetic background (Sv129 × C57BL/6J). All mice were maintained under specific pathogen-free conditions and only late dying mutants (> 100 days) were used for our analyses. All experiments were performed in compliance with the German Law for Welfare of Laboratory Animals.

Genotyping by Southern blot and PCR analysis

For Southern blot analysis, genomic DNA of tail biopsies, skin, muscle, kidney, spleen, liver, dispase separated epidermis and dermis (Sigma, Deisenhofen, Germany) and from macrophages and B-cells was isolated with Easy-DNA™ (Invitrogen, Karlsruhe, Germany). DNA (7.5 μg) was digested with BamHI yielding 2.6 kb fragments for the floxed *Sod2* allele, 7.8 kb for the deleted *Sod2* locus and 8.5 kb for the *Sod2* wild type allele. Bands were detected using a 750 bp HindIII/BamHI fragment of intron2 of *Sod2* allele as a probe. Primer sequences for the PCR-based genotyping for *Sod2* are as follows: P1, 5′-TTA GTA CAT CAT GGC TTG ACG A-3′; P2, 5′-AGG AAA TGC TTT CCC AAC TG-3′ and P3, 5′-GAA AGT CAC CTC CAC ACA CAG A-3′. Primer sequences for the PCR-based genotyping for Cre-recombinase are Cre1, 5′-TTA GCA CCA CGG CAG CAG GAG GTT-3′; Cre2, 5′-CAG GCC AGA TCT CCT GTG CAG CAT-3′. Red-Taq® (Sigma) was used as Taq-Polymerase. PCR samples were subjected to 30 s 94 °C as pre-denaturation, 34 cycles [30 s as annealing (60 °C), 30 s as extension time (72 °C)] and 10 min, 72 °C for final extension.

Reverse transcriptase polymerase chain reaction (RT-PCR)

For RT-PCR, total RNA was isolated from mouse skin using the Trizol method, as described by the manufacturer (Life Technologies, Inc., Rockville, MD, USA). One μg RNA per sample was reverse transcribed using a first strand cDNA reverse transcription-polymerase chain reaction (RT-PCR) synthesis kit (MBI Fermentas, Vilnius, Lithuania). PCR samples were subjected to pre-denaturation (3 min at 94 °C), 21 cycles (30 s at 94 °C, 30 s at 60 °C, 1 min at 72 °C) for GAPDH and 23 cycles for pro-collagen(I) (45 s at 94 °C, 45 s at 60 °C, 1 min at 72 °C) and final extension (10 min at 72 °C). Primers for mouse GAPDH were used as an internal control (forward, 5′- AAG ATT GTC AGC AAT GCA TCC-3′; reverse, 5′- GCC CCT CCT GTT ATT ATG G – 3′) and mouse pro-collagen (I) (forward, 5′-TCG TGA CCG TGA CCT TGC G-3′; reverse, 5′-GAG GCA CAG ACG GCT GAG TAG-3′). PCR products were analysed on a 2.0% agarose gel, followed by quantification by densitometry analysis using TINA2.0 software (TINA; Raytest Isotopenmessgeräte, Straubenhardt, Germany).

Protein lysates and Western blot analysis

Mouse skin was homogenized in ice-cold lysis buffer (50 mM Tris–HCl, pH 7.4, 150 mM NaCl, 2 mM ethylenediamine tetraacetic acid (EDTA), 5 mM phenylmethanesulfonyl fluoride (PMSF), and 1 mM dithiothreitol (DTT), 1% Triton X-100)

with freshly added protease inhibitor cocktail (Roche, Indianapolis, IN, USA). The homogenate was then centrifuged at 15 000 *g* for 30 min at 4 °C, supernatant was collected and aliquots were stored at −70 °C. The protein content in the lysate was determined by the Bradford assay. Equal amounts of protein were subjected to 10% and 12% Tris–Glycine SDS–PAGE gels (as applied), and then transferred onto PVDF membrane. The blot was subsequently blocked with blocking buffer (5% nonfat dry milk, 1% Tween-20 in 20 mM TBS, pH 7.6) for 1 h at room temperature and incubated with monoclonal anti-pro-collagen type I amino-terminal extension peptide antibody (1:1000, SP1.D8; Developmental studies Hybridoma Bank, Iowa, USA), and polyclonal anti-β-actin antibody (1:1000; Chemicon, Temecula, CA, USA), overnight at 4 °C. Thereafter, incubation with a secondary antibody conjugated to horseradish peroxidase (Amersham Life Science, Buckinghamshire, UK) for 1 h at room temperature and detection by ECL system (Amersham, Life Science, Buckinghamshire, UK) was performed. Western blots were also incubated with a primary antibody against Sod2 (FL-222, 1:200; Santa Cruz, CA, USA), actin (CP01, 1:10000; Calbiochem, Gibbstown, NJ, USA), $p16^{INK4a}$ (SC-1661, 1:1000; Santa Cruz) and cleaved (active) caspase-3 (#9664, 1:1000; Cell Signaling Technologies, Danvers, MA, USA) overnight at 4 °C. The secondary antibody goat anti-rabbit conjugated to horseradish peroxidase (for Sod2; IgG, 1:200; Santa Cruz; for actin; IgM, 1:10000; Calbiochem), goat anti-mouse conjugated to horseradish peroxidase (for $p16^{INK4a}$, IgG, 1:10000; Jackson ImmunoResearch Laboratories, Weston, PA, USA) and goat anti-rabbit conjugated to horseradish peroxidase (for caspase-3, Jackson, IgG, 1:10000; ImmunoResearch Laboratories) was incubated for 1 h at room temperature, followed by detection with ECL system (Cell Signaling Technology, Danvers, MA, USA). The detection of carbonylated proteins was performed by Oxyblot™ analysis (S7150; Chemicon) using standard protocols. In brief, protein lysates were derivatized with 2,4-dinitrophenyl hydrazine (DNPH) to add dinitrophenol residue (DNP) into the side chain carbonyl group. As a positive control, oxidized bovine serum albumin (BSA) and as a negative control, reduced BSA were used. Non-derivatized protein lysates were also included to assess the specificity of anti-DNP antibody. All samples were subjected to 10% SDS–PAGE and subsequently transferred onto nitrocellulose membrane and probed with anti-DNP antibody, following incubation with HRP-conjugated secondary antibody. The membrane was then treated with the ECL reagent to visualize the bands.

Fixation procedure for transmission electron microscopy

Mice were anaesthetized subcutaneously by means of Ketamine (100 mg kg^{-1}) and Xylazine (5 mg kg^{-1}) and transcardially perfused with a 2% paraformaldehyde, 2% glutardialdehyde, 0.1 M cacodylate solution buffered at pH 7.35 for 10 min. Thereafter, skin samples were immediately removed and postfixed for further 6–8 h in the same fixative. The samples were then washed three times with 0.1 M cacodylate buffer and stored in this buffer at 4 °C until plastic embedding.

Transmission electron microscopy

Fixed skin samples were cut into small pieces containing both epidermis and dermis. The samples were postfixed with 2% osmium tetraoxide in 0.1 M cacodylate buffer for 2 h at 4 °C. After thorough rinsing in 0.1 M cacodylate buffer for 10 min, slices were dehydrated in a graded ethanol series, and infiltrated with and embedded in araldite. Sections of plastic-embedded specimens were cut with a glass knife for thin sections and a diamond knife for ultra-thin sections on a Reichert ultra-microtome. The 0.5-μm-thin slices were stained with methylene blue and investigated using a Zeiss Axiophot (Zeiss, Oberkochen, Germany). Further contrasting with uranyl acetate–lead citrate was performed and ultrathin 60 nm sections were examined using an electron microscope (902A; Fa. Zeiss).

Histology

Tissues were dissected from the mice and either deep-frozen in O.C.T.™ (Tissue-TEK, Torrance, CA, USA) or fixed overnight in 4% paraformaldehyde in PBS at 4 °C for paraffin embedding. Paraffin sections of 5 μm thickness were used for haematoxylin-eosin and Masson's trichrome staining.

Immunostaining

Cryosections were fixed in 70% ethanol for 10 min at −20 °C and thereafter treated with 0.1% Triton X-100 for 10 min at room temperature. Blocking was performed in 5% BSA for 1 h at 37 °C. Anti-$p16^{INK4a}$ (SC-1661, 1:200; Santa Cruz), Er-TR7 (NB100-64932, 1:200, Novus Biologicals, Cambridge, UK), Sod2 (06-984, 1:200; Millipore, Schwalbach, Germany) and cleaved (active) caspase-3 (#9664, 1:200; Cell Signaling Technologies) as primary antibody were used overnight at 4 °C. Incubation with the secondary antibody Alexa 488 goat anti-rat (for Er-TR7, 1:200), Alexa 555 goat anti-mouse (for $p16^{INK4a}$, 1:200) and Alexa 555 goat anti-rabbit (for Sod2 and caspase-3 1:500) (Invitrogen) was performed for 45 min at room temperature. Isotype control sections were incubated with respective IgG as primary antibodies.

Terminal deoxynucleotidyl transferase dUTP nick end labeling (TUNEL) staining

For *in situ* detection of apoptosis, TUNEL staining was performed using a commercially available kit (*In Situ* Cell Death Detection Kit, POD, Roche, Manheim, Germany) according to the manufacturer's protocol. Briefly, paraffin-embedded skin sections were prepared on glass slides, deparaffinized, rehydrated and treated with Proteinase K. Skin sections were then incu-

bated with labelling solution containing recombinant Terminal deoxynucleotidyl Transferase (TdT) and fluorescein-labelled nucleotides. After washing, sections were counterstained with DAPI and mounted in fluorescence mounting medium (DAKO, Hamburg, Germany) prior to examination by fluorescence microscope (Axio Imager M1; Zeiss) equipped with a green filter.

LacZ reporter mice and X-gal staining

Col1α2-Cre^{+} transgenic mice (B6;129.TgN(Col-Iα2) were bred with ROSA26-LacZ reporter mice (Florin *et al.*, 2004) and the resulting Cre recombinase positive pups (Col1α2-Cre^{+}; ROSA26-LacZ$^{f/+}$) were used to study the site/region of Cre expression. The LacZ gene in ROSA26 locus was kept inactive by placing one 'STOP' codon (flanked by loxP sites on both ends) between the ubiquitous promoter (CMV) and LacZ coding region. Activation of Cre recombinase deleted the 'STOP' codon and thus initiated the expression of β-galactosidase from LacZ gene. Therefore, β-galactosidase would only be expressed in those cells, where cell-specific promoter driven Cre recombinase expression occurred. The mice were first perfused with phosphate-buffered saline (pH 7.4) and later by 4% paraformaldehyde (in phosphate buffered saline, pH 7.4). Different organs, including the skin, intestine, kidney, skeletal muscle, were dissected out and washed with phosphate-buffered saline (pH 7.4) and subjected to mild fixation with 4% paraformaldehyde. The mildly fixed organs were placed in X-gal staining solution (6 mM potassium ferricynide, 6 mM potassium ferrocynide, 2 mM Magnesium chloride, 2.5 mM X-Gal, 0.02% Igepal in phosphate-buffered saline, pH 7.4) and incubated overnight in 37 °C. The stained organs were washed briefly with phosphate-buffered saline (pH 7.4), again fixed with 4% paraformaldehyde and finally processed for paraffin embedding. 5 μm thick paraffin sections were prepared and after counter staining with Nuclear Fast Red (Sigma), the sections were mounted and examined under microscope (Axio Imager M1; Zeiss).

Tail suspension test

This test was performed to assess the motor coordination in mice. Physiologically, when mice are suspended by the tail, they prepare safe landing by actively spreading their hind limbs. Mice were suspended by their tails for 10 s and looked for clasping behaviour of the hind limbs and also the duration of clasping was noted. Hind limb clasping as observed in the mutant mice is indicative of a motor phenotype.

Rotarod

The rotarod test was used to assess motor coordination and balance in rodents (Brooks & Faulkner, 1988). Mice have to keep their balance on a rotating rod (Rotarod Version 1.2.0. MED Associates Inc., Vermont, VT, USA). The time (latency) it takes the mouse to fall off the rod rotating under continuous acceleration (from 4 to 40 rpm in 300 s) was measured. Each mouse had to perform three trials separated by 15 min inter-trial intervals. These trials were averaged.

Determination of muscle fibre diameter

The quadriceps muscle was prepared and subjected to cryopreservation. Cryosections of 10 μm thickness were stained with haematoxylin and eosin (HE). To determine the muscle fibre diameters ($n = 5$ for each group), the standard method for myological diagnostics, the 'lesser fibre diameter' was taken as described previously (Brooke & Engel, 1969). More than 1000 fibres per muscle per mouse with 5000 fibres per genotype were measured at a 20-fold magnification using an Olympus BX51TF microscope equipped with a CCD camera (Soft Imaging System CC12; Olympus, Hamburg Germany) and the Cell^{F} imaging software (Olympus). The fibre measurements from each muscle section were pooled per animal for statistical analysis.

Murine dermal fibroblasts cultivation

New born mice were sacrificed, skin was removed, cut into small pieces digested in a trypsin solution. Single-cell suspension was centrifuged for 5 min at 800 rpm (Heraeus Multifuge 3S-R; Thermo Electron Corporation, Karlsruhe, Germany). The pellet was resuspended in Dulbecco's modified Eagle's medium (Life Technologies, Inc., Eggenstein, Germany) supplemented with 10% foetal calf serum (Biochrom, Berlin, Germany), glutamine (2 mM), penicillin (100 U mL^{-1}) and streptomycin (50 μg mL^{-1}) at 37 °C in a humidified atmosphere. Fibroblasts were cultivated with 3% oxygen and passaged at a 1:2 to 1:3 dilution every 3 days.

Isolation of B-cells

A single cell suspension was prepared from the spleen and B-cells were isolated by labelling with CD19 PE and anti PE Micro Beads (Miltenyi Biotec, Bergisch Galdbach, Germany) for positive selection according to the manufacturer's protocol. Enrichment of > 86% was confirmed by flow cytometry (FACScan; BD Biosciences, Heidelberg, Germany) using an antibody directed against CD45R/B220 PerCP (clone RA3-6B2; BD Biosciences, Pharmingen, Heidelberg, Germany).

Bone marrow-derived macrophages

Bone marrow-derived macrophages (MF) were obtained from femurs as described previously (Sunderkotter *et al.*, 1993). Briefly, bone marrow was flushed through with Dulbecco's minimum essential medium (DMEM) (Biochrom). Following an osmotic-shock, 3×10^6 cells per 10 mL medium were grown in DMEM supplemented with 10% heat-inactivated FCS (PAA Laboratories, Pasching, Austria), 10% conditioned supernatant from L929 cells, 2% L-Glutamine, 1% penicillin/

streptomycin (stock 10 000 U per 10 000 μg mL^{-1}) and 1% non-essential amino acids (Biochrom) in Petri dishes (NUNC, Roskilde, Denmark) in a 7% CO_2 atmosphere at 37 °C. After 6 days, mature macrophages were harvested for DNA extraction.

Bone mineral density (BMD)

High-resolution radiographs were performed on the femurs at 25 kV per 2.2 mA (43805 NX-Ray-System; Hewlett-Packard, Palo Alto, CA, USA) for the visualization of BMD. A quantitative determination was performed using μCT (Fan Beam μ-Scope; Stratec Medical, Pforzheim, Germany). Ten scans with a resolution of 30 μm and with a distance of 30 μm from each other were performed in the proximal right femur (centre of the femoral head). The average BMD was determined for each bone by calculating the mean values of the BMD from 10 scans.

Metabolic cage studies

To assess whether there is any difference in daily food and water consumption among different genotypes of mice, a controlled metabolic cage study was conducted. In this study, mice from each genotype, including mutant, Sod2 heterozygous-deficient and Sod2-competent control mice were caged individually in metabolic chambers (Scanbur, Karlslunde, Denmark) for 3 days under standard conditions. Prior to the actual study, the mice were kept in metabolic cages to adapt themselves. Thereafter, they were kept for further 48 h for the actual analysis. Mice had free access to water and food. The food and water in each cage were changed every day and the remaining food weight and water volume were measured and subtracted from initial values to assess the amount of food and water consumed per 24 h.

Intracellular superoxide anion concentration

Superoxide anions were quantified in fibroblasts using indirect fluorescence with MitoSOX (MitoSOX™ Cat. No. M36008; Invitrogen). MitoSOX is mitochondrial-specific and reaction of superoxide anion in the mitochondria with MitoSOX results in fluorescence emission at 510 nm if excited at 396 nm (Robinson *et al.*, 2006). A concentration dependent curve of MitoSOX fluorescence with increasing concentrations of rotenone in *Sod2*-competent fibroblasts served as a reference. Rotenone is a specific inhibitor of complex I and, thus, causes increased generation of superoxide anion in the mitochondria (Kushnareva *et al.*, 2002). In brief, 1×10^5 fibroblasts were seeded into six well plates and stained with 5 μM MitoSOX for 30 min in the presence and absence of rotenone. After incubation, fibroblasts were washed with HBSS, dislodged by accutase (GmbH; PAA Laboratories, Cölbe, Germany), suspended in 200 μL of HBSS and subjected to fluorescence measurement using a Perkin-Elmer fluorometer for murine dermal fibroblasts (LB 50; Perkin Elmer, Waltham, Massachusetts, USA) or FACSCanto II (BD, Franklin Lakes, NJ, USA) for human dermal fibroblasts.

Detection of mitochondrial H_2O_2 using adenoviral transduction of the genetically encoded fluorescence indicator

The plasmid construct pHyPer-dMito coding for a derivative of the H_2O_2-specific OxyR protein were purchased from Evrogen (Cat.# FP941; Moscow, Russia) (Belousov *et al.*, 2006). The expression cassette was cloned into the adenovirus vector plasmid backbone pGS66 for generation of a replication-deficient E1-deleted adenovirus vector by standard procedures (Schiedner *et al.*, 2000). Cloning details can be obtained upon request. In brief, the vectors were serially amplified on N52.E6 cells and purified by double CsCl-banding. The titres of the vector preparations were determined by a vector genome-based slot-blot procedure (Kreppel *et al.*, 2002) and genome integrity was confirmed by restriction analysis. The replication-deficient adenoviral vector AdMito-HyPer expresses the sensor construct targeted to mitochondria due to the presence of a mitochondrial signal peptide sequence. 1×10^6 *Sod2*-deficient mutant fibroblasts or control fibroblasts were transduced at a multiplicity of infection of 500. Twenty-four hours posttransduction, the mean fluorescence intensity of gated events was measured at 488 nm for FITC and 405 nm for AmCyan by flow cytometry (FACS Canto II; BD Biosciences) and evaluated considering both the autofluorescence (AF) and the number of events in each gate (Ev) as given in the formula below. Transduced fibroblasts were also analysed with a fluorescence microscope (Axiovert 200M; Zeiss).

Statistical calculations

The exact two-sample Wilcoxon test or one-way ANOVA were used to compare independent measurements between control, heterozygous, mutant and old mice. For repeated comparison at different time points, a correction of the *P*-values according to Bonferroni (i.e. multiplication of each *P*-value by the number of time points) was performed. For comparisons of survival times, the log-rank test was applied, optionally stratified for gender. All tests were two-sided. Calculations were performed using the SAS software, version 9.1 (SAS Institute Inc., Cary, NC, USA).

$$Ratio = \frac{\frac{FITC_{gate1} - FITC_{AF}}{AmCyan_{gate1} - AmCyan_{AF}} * Ev_{gate1} + \frac{FITC_{gate2} - FITC_{AF}}{AmCyan_{gate2} - AmCyan_{AF}} * Ev_{gate2}}{Ev_{gate1} + Ev_{gate2}}$$

Acknowledgments

AL, SI, MB and KS-K are supported by the German Research Foundation within the Clinical Research Group KFO142: 'Cellular and Molecular Mechanisms of Ageing – From Mechanisms to Clinical Perspectives'. MW and KS-K are supported by the European Union through the Integrated Project PROTEOMAGE (FP6-518230). AS and KS-K received a grant from the German

Research Foundation within the Collaborative Research Centre SFB 497: 'Signals and Signal Processing during Cellular Differentiation'. JHC is supported by the Korea Science and Engineering Foundation (KOSEF) through the Centre for Aging and Apoptosis Research at Seoul National University (R11-2002-097-06001-0). We are grateful to HJ Fehling for providing the RFP indicator mice and to P. Angel for providing the Col1α2-Cre mice.

Author contributions

Nicolai Treiber generated and characterized the phenotypes of mutant mice. Pallab Maity, Karmveer Singh characterized the phenotype of the mutant mice and were involved in data collection, analysis, interpretation and assembly. Matthias Kohn analysed the genetic basis of the mutant mice. Florentina Ferchiu and Lea Sante contributed data on enhanced superoxide anion levels in senescent human fibroblasts. Meinhard Wlaschek, Wilhelm Bloch, Sebastian Iben, Anca Sindrilaru, Mark Berneburg, Albert Ludolph contributed to the concept and design and approval of the manuscript. Alexander F. Keist. Sebastian Frese, Michael Ohnmacht, Josef Högel, Jin Ho Chung, Min Jung Lee, York Karmenich, Kerstin Braunstein contributed to data collection, and analysis. Lutz Claes, Anita Ignatius, Thorsten Nikolaus, Anne-Dorte Sperfeld added knowledge on translation of our murine data to human diseases. Karlis Briviba, Florian Kreppel and Stefan Kochanek provided the techniques for mitochondrial-specific H_2O_2 quantification, data analysis and interpretation. Karin Scharffetter-Kochanek is responsible for the concept, design, collection and assembly of data, data interpretation, manuscript writing and final approval of the manuscript.

References

Allen RG, Tresini M, Keogh BP, Doggett DL, Cristofalo VJ (1999) Differences in electron transport potential, antioxidant defenses, and oxidant generation in young and senescent fetal lung fibroblasts (WI-38). *J. Cell. Physiol.* **180**, 114–122.

Belousov VV, Fradkov AF, Lukyanov KA, Staroverov DB, Shakhbazov KS, Terskikh AV, Lukyanov S (2006) Genetically encoded fluorescent indicator for intracellular hydrogen peroxide. *Nat. Methods* **3**, 281–286.

Bodine PV, Billiard J, Moran RA, Ponce-de-Leon H, McLarney S, Mangine A, Scrimo MJ, Bhat RA, Stauffer B, Green J, Stein GS, Lian JB, Komm BS (2005) The Wnt antagonist secreted frizzled-related protein-1 controls osteoblast and osteocyte apoptosis. *J. Cell. Biochem.* **96**, 1212–1230.

Brooke MH, Engel WK (1969) The histographic analysis of human muscle biopsies with regard to fiber types. 2. Diseases of the upper and lower motor neuron. *Neurology* **19**, 378–393.

Brooks SV, Faulkner JA (1988) Contractile properties of skeletal muscles from young, adult and aged mice. *J. Physiol.* **404**, 71–82.

Campisi J (2005) Senescent cells, tumor suppression, and organismal aging: good citizens, bad neighbors. *Cell* **120**, 513–522.

Coppe JP, Patil CK, Rodier F, Sun Y, Munoz DP, Goldstein J, Nelson PS, Desprez PY, Campisi J (2008) Senescence-associated secretory phenotypes reveal cell-nonautonomous functions of oncogenic RAS and the p53 tumor suppressor. *PLoS Biol.* **6**, 2853–2868.

Cummings SR, Melton LJ (2002) Epidemiology and outcomes of osteoporotic fractures. *Lancet* **359**, 1761–1767.

Dai CY, Enders GH (2000) p16 INK4a can initiate an autonomous senescence program. *Oncogene* **19**, 1613–1622.

Ferrari SL, Deutsch S, Choudhury U, Chevalley T, Bonjour JP, Dermitzakis ET, Rizzoli R, Antonarakis SE (2004) Polymorphisms in the low-density lipoprotein receptor-related protein 5 (LRP5) gene are associated with variation in vertebral bone mass, vertebral bone size, and stature in whites. *Am. J. Hum. Genet.* **74**, 866–875.

Fisher AL (2004) Of worms and women: sarcopenia and its role in disability and mortality. *J. Am. Geriatr. Soc.* **52**, 1185–1190.

Fisher GJ, Varani J, Voorhees JJ (2008) Looking older: fibroblast collapse and therapeutic implications. *Arch. Dermatol.* **144**, 666–672.

Florin L, Alter H, Grone HJ, Szabowski A, Schutz G, Angel P (2004) Cre recombinase-mediated gene targeting of mesenchymal cells. *Genesis* **38**, 139–144.

Garinis GA (2008) Nucleotide excision repair deficiencies and the somatotropic axis in aging. *Hormones (Athens)* **7**, 9–16.

Garinis GA, van der Horst GT, Vijg J, Hoeijmakers JH (2008) DNA damage and ageing: new-age ideas for an age-old problem. *Nat. Cell Biol.* **10**, 1241–1247.

Gerhard GS, Kasales CJ (2003) Aging and kyphosis. *J. Gerontol. A Biol. Sci. Med. Sci.* **58**, 968.

Grillari J, Katinger H, Voglauer R (2007) Contributions of DNA interstrand cross-links to aging of cells and organisms. *Nucleic Acids Res.* **35**, 7566–7576.

Haines DC, Chattopadhyay S, Ward JM (2001) Pathology of aging B6;129 mice. *Toxicol. Pathol.* **29**, 653–661.

Hiona A, Leeuwenburgh C (2008) The role of mitochondrial DNA mutations in aging and sarcopenia: implications for the mitochondrial vicious cycle theory of aging. *Exp. Gerontol.* **43**, 24–33.

Horowitz MC, Lorenzo JA (2007) Immunologic regulation of bone development. *Adv. Exp. Med. Biol.* **602**, 47–56.

Huang TT, Naeemuddin M, Elchuri S, Yamaguchi M, Kozy HM, Carlson EJ, Epstein CJ (2006) Genetic modifiers of the phenotype of mice deficient in mitochondrial superoxide dismutase. *Hum. Mol. Genet.* **15**, 1187–1194.

Hutter E, Unterluggauer H, Uberall F, Schramek H, Jansen-Durr P (2002) Replicative senescence of human fibroblasts: the role of Ras-dependent signaling and oxidative stress. *Exp. Gerontol.* **37**, 1165–1174.

Iannuzzi-Sucich M, Prestwood KM, Kenny AM (2002) Prevalence of sarcopenia and predictors of skeletal muscle mass in healthy, older men and women. *J. Gerontol. A Biol. Sci. Med. Sci.* **57**, M772–M777.

Jang YC, Lustgarten MS, Liu Y, Muller FL, Bhattacharya A, Liang H, Salmon AB, Brooks SV, Larkin L, Hayworth CR, Richardson A, Van Remmen H (2010) Increased superoxide *in vivo* accelerates age-associated muscle atrophy through mitochondrial dysfunction and neuromuscular junction degeneration. *FASEB J.* **24**, 1376–1390.

Kalu DN (1995) *Handbook of Physiology: Section 11: Aging: Aging Section 11. In Handbook of Physiology: Section 11: Aging: Aging Section 11 (Handbook of Physiology)*. USA: Oxford University Press Inc.

Kaya G, Tran C, Sorg O, Hotz R, Grand D, Carraux P, Didierjean L, Stamenkovic I, Saurat JH (2006) Hyaluronate fragments reverse skin atrophy by a CD44-dependent mechanism. *PLoS Med* **3**, e493.

Kim WY, Sharpless NE (2006) The regulation of INK4/ARF in cancer and aging. *Cell* **127**, 265–275.

Kim JV, Kang SS, Dustin ML, McGavern DB (2009) Myelomonocytic cell recruitment causes fatal CNS vascular injury during acute viral meningitis. *Nature* **457**, 191–195.

Kops GJ, Dansen TB, Polderman PE, Saarloos I, Wirtz KW, Coffer PJ, Huang TT, Bos JL, Medema RH, Burgering BM (2002) Forkhead tran-

scription factor FOXO3a protects quiescent cells from oxidative stress. *Nature* **419**, 316–321.

Kreppel F, Biermann V, Kochanek S, Schiedner G (2002) A DNA-based method to assay total and infectious particle contents and helper virus contamination in high-capacity adenoviral vector preparations. *Hum. Gene Ther.* **13**, 1151–1156.

Krishnamurthy J, Torrice C, Ramsey MR, Kovalev GI, Al-Regaiey K, Su L, Sharpless NE (2004) Ink4a/Arf expression is a biomarker of aging. *J. Clin. Invest.* **114**, 1299–1307.

Krishnamurthy J, Ramsey MR, Ligon KL, Torrice C, Koh A, Bonner-Weir S, Sharpless NE (2006) p16INK4a induces an age-dependent decline in islet regenerative potential. *Nature* **443**, 453–457.

Krtolica A, Campisi J (2002) Cancer and aging: a model for the cancer promoting effects of the aging stroma. *Int. J. Biochem. Cell Biol.* **34**, 1401–1414.

Kushnareva Y, Murphy AN, Andreyev A (2002) Complex I-mediated reactive oxygen species generation: modulation by cytochrome c and NAD(P)+ oxidation-reduction state. *Biochem. J.* **368**, 545–553.

Labat-Robert J, Robert L (2007) The effect of cell-matrix interactions and aging on the malignant process. *Adv. Cancer Res.* **98**, 221–259.

Larsson L (1978) Morphological and functional characteristics of the ageing skeletal muscle in man. A cross-sectional study. *Acta Physiol. Scand. Suppl.* **457**, 1–36.

Lass A, Sohal BH, Weindruch R, Forster MJ, Sohal RS (1998) Caloric restriction prevents age-associated accrual of oxidative damage to mouse skeletal muscle mitochondria. *Free Radic. Biol. Med.* **25**, 1089–1097.

Lebovitz RM, Zhang H, Vogel H, Cartwright J Jr, Dionne L, Lu N, Huang S, Matzuk MM (1996) Neurodegeneration, myocardial injury, and perinatal death in mitochondrial superoxide dismutase-deficient mice. *Proc. Natl. Acad. Sci. U S A* **93**, 9782–9787.

Lee SS, Kennedy S, Tolonen AC, Ruvkun G (2003) DAF-16 target genes that control C. elegans life-span and metabolism. *Science* **300**, 644–647.

Li Y, Huang TT, Carlson EJ, Melov S, Ursell PC, Olson JL, Noble LJ, Yoshimura MP, Berger C, Chan PH, Wallace DC, Epstein CJ (1995) Dilated cardiomyopathy and neonatal lethality in mutant mice lacking manganese superoxide dismutase. *Nat. Genet.* **11**, 376–381.

Luche H, Weber O, Nageswara Rao T, Blum C, Fehling HJ (2007) Faithful activation of an extra-bright red fluorescent protein in ''knock-in'' Cre-reporter mice ideally suited for lineage tracing studies. *Eur. J. Immunol.* **37**, 43–53.

Ma W, Wlaschek M, Tantcheva-Poor I, Schneider LA, Naderi L, Razi-Wolf Z, Schuller J, Scharffetter-Kochanek K (2001) Chronological ageing and photoageing of the fibroblasts and the dermal connective tissue. *Clin. Exp. Dermatol.* **26**, 592–599.

Marzetti E, Lees HA, Wohlgemuth SE, Leeuwenburgh C (2009) Sarcopenia of aging: underlying cellular mechanisms and protection by calorie restriction. *Biofactors* **35**, 28–35.

Metter EJ, Talbot LA, Schrager M, Conwit R (2002) Skeletal muscle strength as a predictor of all-cause mortality in healthy men. *J. Gerontol. A Biol. Sci. Med. Sci.* **57**, B359–B365.

Molofsky AV, Slutsky SG, Joseph NM, He S, Pardal R, Krishnamurthy J, Sharpless NE, Morrison SJ (2006) Increasing p16INK4a expression decreases forebrain progenitors and neurogenesis during ageing. *Nature* **443**, 448–452.

Muller FL, Lustgarten MS, Jang Y, Richardson A, Van Remmen H (2007) Trends in oxidative aging theories. *Free Radic. Biol. Med.* **43**, 477–503.

Newton-John HF, Morgan DB (1970) The loss of bone with age, osteoporosis, and fractures. *Clin. Orthop. Relat. Res.* **71**, 229–252.

Niedernhofer LJ, Garinis GA, Raams A, Lalai AS, Robinson AR, Appeldoorn E, Odijk H, Oostendorp R, Ahmad A, van Leeuwen W, Theil AF, Vermeulen W, van der Horst GT, Meinecke P, Kleijer WJ, Vijg J, Jaspers NG, Hoeijmakers JH (2006) A new progeroid syndrome reveals that genotoxic stress suppresses the somatotroph axis. *Nature* **444**, 1038–1043.

Oikarinen A (1994) Aging of the skin connective tissue: how to measure the biochemical and mechanical properties of aging dermis. *Photodermatol. Photoimmunol. Photomed.* **10**, 47–52.

Perrini S, Laviola L, Carreira MC, Cignarelli A, Natalicchio A, Giorgino F (2010) The GH/IGF1 axis and signaling pathways in the muscle and bone: mechanisms underlying age-related skeletal muscle wasting and osteoporosis. *J. Endocrinol.* **205**, 201–210.

Petrie HT, Van Ewijk W (2002) Thymus by numbers. *Nat. Immunol.* **3**, 604–605.

van der Pluijm I, Garinis GA, Brandt RM, Gorgels TG, Wijnhoven SW, Diderich KE, de Wit J, Mitchell JR, van Oostrom C, Beems R, Niedernhofer LJ, Velasco S, Friedberg EC, Tanaka K, van Steeg H, Hoeijmakers JH, van der Horst GT (2007) Impaired genome maintenance suppresses the growth hormone–insulin-like growth factor 1 axis in mice with Cockayne syndrome. *PLoS Biol.* **5**, e2.

Quan T, Shao Y, He T, Voorhees JJ, Fisher GJ (2010) Reduced expression of connective tissue growth factor (CTGF/CCN2) mediates collagen loss in chronologically aged human skin. *J. Invest. Dermatol.* **130**, 415–424.

Raisz LG (2005) Pathogenesis of osteoporosis: concepts, conflicts, and prospects. *J. Clin. Invest.* **115**, 3318–3325.

Ralston SH, de Crombrugghe B (2006) Genetic regulation of bone mass and susceptibility to osteoporosis. *Genes Dev.* **20**, 2492–2506.

Rantanen T, Guralnik JM, Foley D, Masaki K, Leveille S, Curb JD, White L (1999) Midlife hand grip strength as a predictor of old age disability. *JAMA* **281**, 558–560.

Ressler S, Bartkova J, Niederegger H, Bartek J, Scharffetter-Kochanek K, Jansen-Durr P, Wlaschek M (2006) p16INK4A is a robust *in vivo* biomarker of cellular aging in human skin. *Aging Cell* **5**, 379–389.

Robinson KM, Janes MS, Pehar M, Monette JS, Ross MF, Hagen TM, Murphy MP, Beckman JS (2006) Selective fluorescent imaging of superoxide *in vivo* using ethidium-based probes. *Proc. Natl. Acad. Sci. U S A* **103**, 15038–15043.

Scharffetter-Kochanek K, Wlaschek M, Brenneisen P, Schauen M, Blaudschun R, Wenk J (1997) UV-induced reactive oxygen species in photocarcinogenesis and photoaging. *Biol. Chem.* **378**, 1247–1257.

Schiedner G, Hertel S, Kochanek S (2000) Efficient transformation of primary human amniocytes by E1 functions of Ad5: generation of new cell lines for adenoviral vector production. *Hum. Gene Ther.* **11**, 2105–2116.

Shin MH, Rhie GE, Kim YK, Park CH, Cho KH, Kim KH, Eun HC, Chung JH (2005) H2O2 accumulation by catalase reduction changes MAP kinase signaling in aged human skin *in vivo*. *J. Invest. Dermatol.* **125**, 221–229.

Sies H (1986) Biochemistry of Oxidative Stress. *Angew. Chem. Int. Ed. Engl.* **25**, 1058–1071.

Sies H (1991) *Oxidative Stress: Oxidants and Antioxidants*. New York: Academic Press,Inc.

Stessman J, Maaravi Y, Hammerman-Rozenberg R, Cohen A, Nemanov L, Gritsenko I, Gruberman N, Ebstein RP (2005) Candidate genes associated with ageing and life expectancy in the Jerusalem longitudinal study. *Mech. Ageing Dev.* **126**, 333–339.

Strassburger M, Bloch W, Sulyok S, Schuller J, Keist AF, Schmidt A, Wenk J, Peters T, Wlaschek M, Lenart J, Krieg T, Hafner M, Kumin A, Werner S, Muller W, Scharffetter-Kochanek K (2005) Heterozygous deficiency of manganese superoxide dismutase results in severe lipid peroxidation and spontaneous apoptosis in murine myocardium *in vivo*. *Free Radic. Biol. Med.* **38**, 1458–1470.

Sunderkotter C, Kunz M, Steinbrink K, Meinardus-Hager G, Goebeler M, Bildau H, Sorg C (1993) Resistance of mice to experimental leishmaniasis is associated with more rapid appearance of mature macrophages *in vitro* and *in vivo*. *J. Immunol.* **151**, 4891–4901.

Szabo C, Ischiropoulos H, Radi R (2007) Peroxynitrite: biochemistry, pathophysiology and development of therapeutics. *Nat. Rev. Drug Discov.* **6**, 662–680.

Szulc P, Beck TJ, Marchand F, Delmas PD (2005) Low skeletal muscle mass is associated with poor structural parameters of bone and impaired balance in elderly men–the MINOS study. *J. Bone Miner. Res.* **20**, 721–729.

Tasker PN, Albagha OM, Masson CB, Reid DM, Ralston SH (2004) Association between TNFRSF1B polymorphisms and bone mineral density, bone loss and fracture. *Osteoporos. Int.* **15**, 903–908.

Treiber N, Peters T, Sindrilaru A, Huber R, Kohn M, Menke A, Briviba K, Kreppel F, Basu A, Maity P, Koller M, Iben S, Wlaschek M, Kochanek S, Scharffetter-Kochanek K (2009) Overexpression of manganese superoxide dismutase in human dermal fibroblasts enhances the contraction of free floating collagen lattice: implications for ageing and hyperplastic scar formation. *Arch. Dermatol. Res.* **301**, 273–287.

Usuki F, Yasutake A, Umehara F, Higuchi I (2004) Beneficial effects of mild lifelong dietary restriction on skeletal muscle: prevention of age-related mitochondrial damage, morphological changes, and vulnerability to a chemical toxin. *Acta Neuropathol.* **108**, 1–9.

Valenti L, Conte D, Piperno A, Dongiovanni P, Fracanzani AL, Fraquelli M, Vergani A, Gianni C, Carmagnola L, Fargion S (2004) The mitochondrial superoxide dismutase A16V polymorphism in the cardiomyopathy associated with hereditary haemochromatosis. *J. Med. Genet.* **41**, 946–950.

Van Remmen H, Jones DP (2009) Current thoughts on the role of mitochondria and free radicals in the biology of aging. *J. Gerontol. A Biol. Sci. Med. Sci.* **64**, 171–174.

Van Remmen H, Ikeno Y, Hamilton M, Pahlavani M, Wolf N, Thorpe SR, Alderson NL, Baynes JW, Epstein CJ, Huang TT, Nelson J, Strong R, Richardson A (2003) Life-long reduction in MnSOD activity results in increased DNA damage and higher incidence of cancer but does not accelerate aging. *Physiol. Genomics* **16**, 29–37.

Wallace DC (2010) Mitochondrial DNA mutations in disease and aging. *Environ. Mol. Mutagen.* **51**, 440–450.

Wallace DC, Brown MD, Lott MT (1999) Mitochondrial DNA variation in human evolution and disease. *Gene* **238**, 211–230.

Wenk J, Brenneisen P, Wlaschek M, Poswig A, Briviba K, Oberley TD, Scharffetter-Kochanek K (1999) Stable overexpression of manganese superoxide dismutase in mitochondria identifies hydrogen peroxide as a major oxidant in the AP-1-mediated induction of matrix-degrading metalloprotease-1. *J. Biol. Chem.* **274**, 25869–25876.

Wenk J, Schuller J, Hinrichs C, Syrovets T, Azoitei N, Podda M, Wlaschek M, Brenneisen P, Schneider LA, Sabiwalsky A, Peters T, Sulyok S, Dissemond J, Schauen M, Krieg T, Wirth T, Simmet T, Scharffetter-Kochanek K (2004) Overexpression of phospholipid-hydroperoxide glutathione peroxidase in human dermal fibroblasts abrogates UVA irradiation-induced expression of interstitial collagenase/matrix metalloproteinase-1 by suppression of phosphatidylcholine hydroperoxide-mediated NFkappaB activation and interleukin-6 release. *J. Biol. Chem.* **279**, 45634–45642.

Zofkova I (2003) Pathophysiological and clinical importance of insulin-like growth factor-I with respect to bone metabolism. *Physiol. Res.* **52**, 657–679.

Supporting Information

Additional supporting information may be found in the online version of this article:

Fig. S1 Generation of the mutant mice with severe aging phenotype.

Fig. S2 Analysis of feeding and drinking pattern of early and late dying mutant mice.

Fig. S3 Analysis of apoptosis in the hearts of early and late dying mutant mice.

Fig. S4 Analysis of vertical diameter or thickness of different layers of skin.

Fig. S5 Specificity of *Col1α2-Cre* using ROSA26 LacZ reporter mice.

Fig. S6 Fibroblast-specific deletion of Sod2 in the skin and skeletal muscle.

Fig. S7 Enhanced superoxide anion generation in replicative senescent human dermal fibroblasts.

Data S1 Generation of the mutant phenotype.

As a service to our authors and readers, this journal provides supporting information supplied by the authors. Such materials are peer-reviewed and may be re-organized for online delivery, but are not copy-edited or typeset. Technical support issues arising from supporting information (other than missing files) should be addressed to the authors.